To cite this paper: W. Fei, P. C. K. Luk, J. X. Shen, B. Xia, and Y. Wang, "Permanent magnet flux switching integrated-starter-generator with different rotor configurations for cogging torque and torque ripple mitigations," IEEE Transactions on Industry Applications, vol.47, no.3, pp.1247-1256, 2011.

Permanent Magnet Flux Switching Integrated-Starter-Generator with Different Rotor Configurations for Cogging Torque and Torque Ripple Mitigations

W. Fei, P. C. K. Luk, *Senior Member*, *IEEE*, J. X. Shen, *Senior Member*, *IEEE*, B. Xia, and Y. Wang

***Abstract*—This paper investigates the cogging torque and torque ripple features of a permanent magnet flux switching (PMFS) integrated-starter-generator (ISG). The effects of the rotor pole arc width on cogging torque, torque ripple and output torque are first established using finite element analysis (FEA). Three torque ripple reduction techniques based on the optimization of three different rotor pole configurations – uniform, step skewed and axial pairing, are then proposed. The torque characteristics of each rotor configuration at varying load currents and phase angles are studied in detail. A prototype machine with a common stator and the three optimized rotor configurations are built for experimental validation. Both the FEA results and the experimental tests show that the step skewed and axial pairing techniques can alleviate the cogging torque significantly but the latter is less effective than the former in reducing the overall torque ripple.**

***Index Terms*—Axial pairing, back EMF, cogging torque, finite element analysis, phase angle, reluctance torque, step skew, torque ripple.**

I. Introduction

THE EARLY LITERATURE on permanent magnet flux switching (PMFS) machines can be dated back to the 1950s [1]. Yet only since last decade has seen some revived interests on the machine due to a multitude of reasons including advances in rare earth permanent magnet (PM) materials, emergence of sophisticated computer-aided motor design tools, and the quest for better machines [2]-[6]. In general, today's PMFS machines have distinctive merits such as high torque density, good flux weakening capability, simple thermal management, and mechanical robustness. Both nonlinear lumped parameter magnetic circuit and finite element analysis (FEA) models have been developed to evaluate and validate these advantages [7]-[10]. Meanwhile, PMFS machines with different configurations have been proposed for a wide range of applications, from low power axial fans [11] to oil breathers [12], and from traction [13,14] to more-electric aircraft [15].

The integrated-starter-generator (ISG) is considered a preferred configuration over the conventional separated starter-generator set in modern automotive applications [16]. The critical requirements such as extremely high starting torque for cold cranking and constant voltage output over a very wide speed range for battery charging, have underpinned the PMFS machine as a potential candidate for ISG applications. Recently, a new ISG has been proposed to harness the unique features of the PMFS machine [17]. However, cogging torque and torque pulsation, which are of particular importance for ISG, of the PMFS machine are rather high compared with other PM machines. This is due to the doubly salient structure, high air gap flux density and magnetic saturations in the stator core. As yet, there are relatively exiguous studies on the cogging torque and torque ripple optimizations from either machine design [18-21] or control [22] perspectives. Normally, techniques based on machine design are more effective than the control based ones. This is because machine design can minimize cogging torque as well as optimize back EMF and hence torque ripples, by means of optimization of the machine's geometric parameters, whereas machine control usually involves precise excitation of current profiles based on complex real-time computations and is highly dependent of the reliability and accuracy of the sensors used. In PMFS machines, both the armature windings and permanent magnets are located in the stator, and the passive rotor is formed by stacked lamination sheets similar to that of the switched reluctance machine (SRM). Therefore, it is usually more preferable to adopt torque ripple reduction techniques from the rotor design perspective for cost-effective implementation.

In this paper, the main specifications of the PMFS machine under study are first introduced and the modeling approach is discussed. Then the effects of the rotor pole arc width (RPAW) on cogging torque, torque ripple and output torque are established using two-dimensional (2-D) FEA. Three different rotor configurations — optimal RPAW with uniform rotor teeth, rotor step skewed (RSS) and rotor teeth axial pairing (RTAP), are proposed to mitigate the cogging torque and torque pulsations. The torque characteristics of each configuration at varying load currents and phase angles (electrical degree) are obtained by the 2-D FEA modeled.

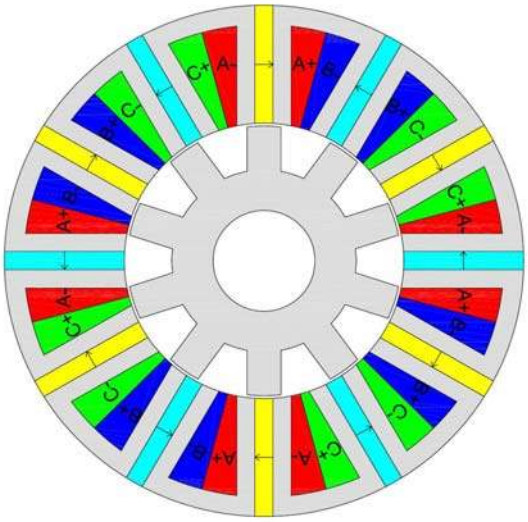

Fig. 1. Schematic of the proposed PMFS ISG.

TABLE I
MAIN DESIGN PARAMETERS OF THE MACHINE

Symbol	Machine Parameter	Values	Unit
p	Phase number	3	-
N_s	Stator pole number	12	-
N_r	Rotor pole number	10	-
N	Coil turn number	6	-
PM	Magnet material	NdFeB35	-
R_{so}	Stator outer radius	46.00	mm
R_{ro}	Rotor outer radius	24.75	mm
g	Air gap length	0.50	mm
h_{pm}	Magnet thickness	3.24	mm
h_{pr}	Rotor tooth height	6.06	mm
l_a	Machine stack length	60	mm
n_r	Rated rotational speed	1000	rpm
T_{ra}	Rated output torque	5.5	N·m
I_r	Rated phase current	50 (peak)	A
U_{dc}	DC link Voltage	12	V

Furthermore, three-dimensional (3-D) FEA models are developed to account for both the end effects and the axially-coupling effects between rotor teeth, and to validate the 2-D FEA results. Finally, a prototype machine with a common stator and the three optimized rotor configurations are built. Comprehensive experimental tests are undertaken to validate the predicted results from the FEA models. Using the optimized RPAW configuration with uniform rotor teeth as the benchmark, the results show that the RSS method could significantly reduce both the cogging torque and torque ripple. On the other hand, the newly proposed RTAP technique can effectively mitigate the cogging torque but is not particularly useful to suppress the overall torque pulsation.

II. PMFS ISG AND MODELING

The proposed PMFS ISG comprises a complex stator of 12 poles with embedded PMs and concentrated coils and a simple and passive rotor of 10 poles, as shown in the schematic in Fig.1. Whilst the overall design and analysis of the machine have been reported in the previous study [17], the main design parameters of the machine, to which the proposed torque ripple reduction techniques relate, are given in Table I.

Generally, the torque output of a PMFS machine can be derived by principle of virtual work as

$$\begin{aligned} T &= \frac{\partial W_{coenergy}(i,\theta)}{\partial \theta}\Big|_{i=\text{constant}} \\ &= \frac{\partial \left(i^T \lambda(i,\theta) - W_{field}(i,\theta)\right)}{\partial \theta}\Big|_{i=\text{constant}} \end{aligned} \tag{1}$$

where $W_{coenergy}(i,\theta)$, $\lambda(i,\theta)$ and $W_{field}(i,\theta)$ are the corresponding co-energy, flux linkage and field energy of the machine with certain excitation current i and rotor position θ respectively. By ignoring magnetic saturation in the machine, the flux linkage and field energy can be decoupled and equation (1) can therefore be rewritten as

$$\begin{aligned} T &= i^T \frac{d\lambda_{pm}(\theta)}{d\theta} + \frac{1}{2} i^T \frac{\partial L(\theta)}{d\theta} i - \frac{dW_{pm}(\theta)}{d\theta} \\ &= T_{pm} + T_r + T_{cogging} \end{aligned} \tag{2}$$

where $\lambda_{pm}(\theta)$, $L(\theta)$ and $W_{pm}(\theta)$ are the corresponding PM flux linkage, inductance and PM field energy at rotor position θ respectively, T_{pm} is the torque generated by interaction between the magnetic fields by winding current i and the PMs, T_r is the reluctance torque produced by winding inductance variations with rotor position, and $T_{cogging}$ is cogging torque caused the PM field energy alterations with rotor position. It can be inspected that the instantaneous torque of the machine is an aggregate of three parts, so is its torque ripple. However, saturations inevitably exist in both stator and rotor of PMFS machine [7], which would make decomposition of the parts contributing to the output torque unfeasible. Furthermore, since the PMFS machine has essentially sinusoidal back EMF, it is particularly suitable for brushless AC mode of operation for minimum torque ripple [2], [7]. For analysis in this paper, it is assumed that the machine is excited by pure sinusoidal current.

III. ROTOR POLE ARC WIDTH

The analysis and optimization of back EMF in a PMFS machine with a common stator and varying rotor pole combinations have been carried out through RPAW design [22]. It is also found that while the RPAW can greatly influence the cogging torque and torque ripple of the machine, an optimum value is always obtainable subject to the requirements of a given application [7]. This, however, would invariably lead to compromise between the magnitude and quality of the output torque.

In this paper, the RPAW is normalized to stator permanent magnet arc width for clarity in analysis. The cogging torque waveforms for the machine with different RPAW are computed by 2-D FEA and depicted in Fig. 2. However, the PMFS machine has a unique doubly salient structure so that the direct-axis reluctance is larger than quadrature-axis one [14], [24]. Thus, current phase advancing should be implemented in order to generate the maximum possible torque. Under

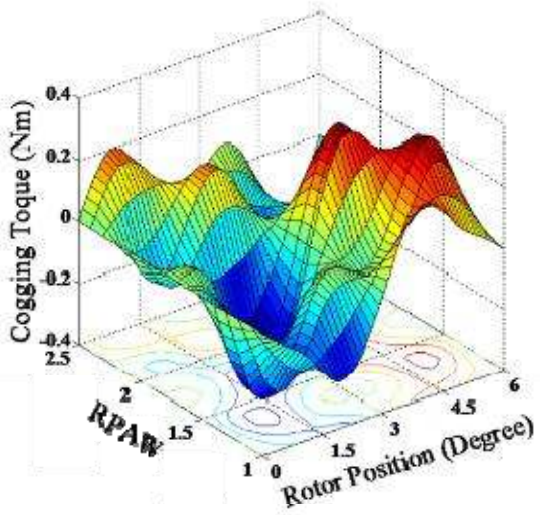

Fig. 2. Cogging torque profiles with different RPAW.

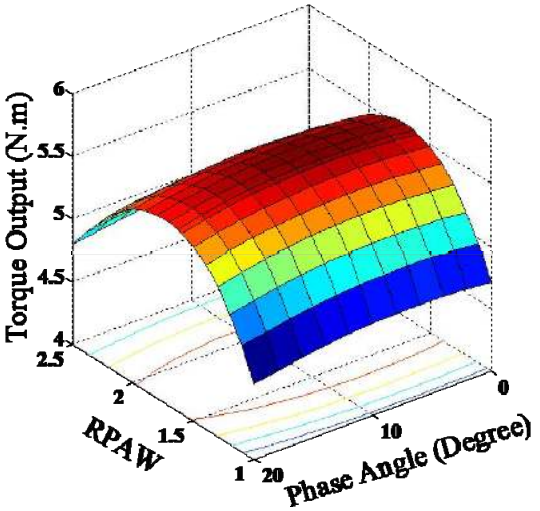

Fig. 3. Torque output variations with different current phase advance angles and RPAW.

values of the machine with different RPAW and current phase advance angle ranged from 0 to 20 electrical degree are evaluated as shown in Fig. 3, which shows the current phase advance angle for maximum output torque is about 8 degrees. Thus, at 8 degrees phase advancing operation, the corresponding torque amplitudes, peak-to-peak (P-P) torque ripple and cogging torque for different RPAW are illustrated in Fig. 4, which shows the optimal RPAW is 1.7 for maximum torque, and 1.9 for minimum torque ripple.

From Fig.4, it is evident that RPAW greatly affects both the cogging torque and torque ripples, and hence the output torque. It should be noted, though less explicit in their characteristics curves, that cogging torque and torque ripples in the machine can either counteract or aggravate with each other [25]. This observation comports with the results in Fig. 4 that the P-P cogging torque values are larger than the P-P torque ripple ones when RPAW is less than 1.9, but smaller when RPAW exceeds

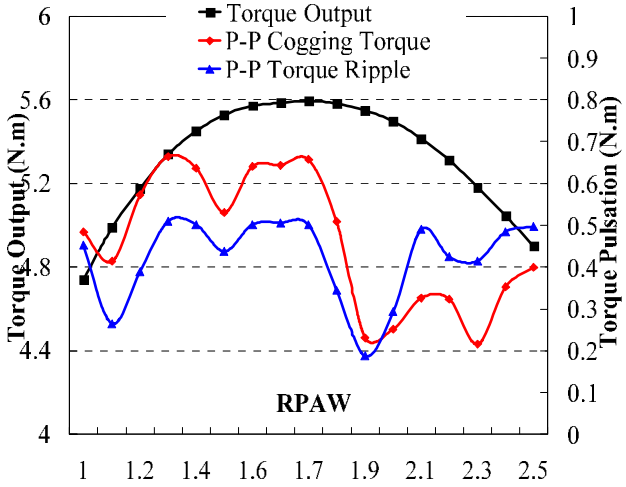

Fig. 4. Torque amplitude, P-P cogging torque and torque ripple variations with different RPAW.

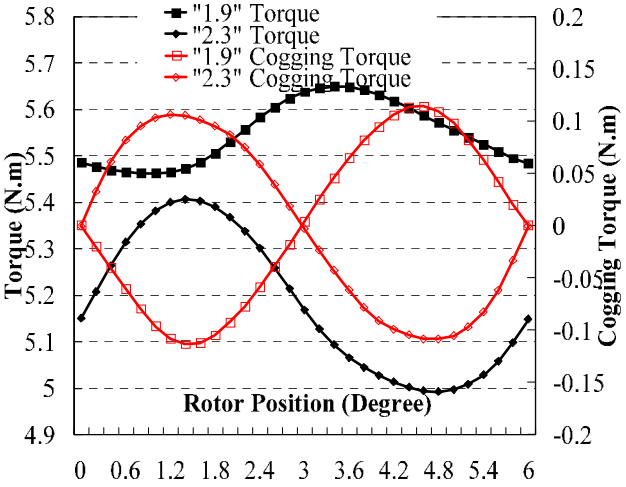

Fig. 5. Output torque and cogging torque profiles with 1.9 and 2.3 RPAW.

overall torque pulsation optimization, and forms the basis for the proposed teeth pairing configuration. In Fig.5, the output torque and cogging torque profiles at 1.9 and 2.3 RPAW are shown. Although the two RPAW values both produce a similar minimum cogging torque of 0.2Nm (peak), they have opposing polarities. The results in Fig.5 show that 1.9 RPAW produces a higher output torque with less torque pulsations. This can further be explained by the characteristic cruves in Fig.4, which shows the torque ripple is lower than the cogging torque with 1.9 RPAW, but is at 0.4Nm (peak) which is twice the cogging torque value with 2.3 RPAW.

IV. Different Rotor Configurations for Cogging Torque Reduction

The merit of a cogging torque reduction technique generally depends on complexity and hence the cost of implementation and its impact on output torque and other machine performance. Due to the relatively complex structure of the stator of the proposed PMFS machine, cogging torque reduction techniques

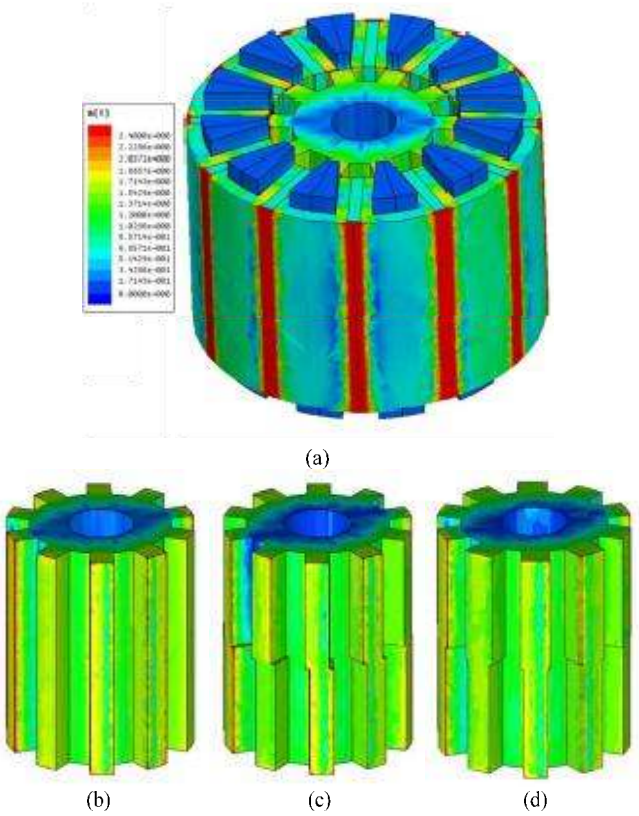

Fig. 6. The proposed PMFS machine with three rotor configurations: (a) stator and rotor, (b) uniform rotor with 1.9 RPAW, (c) rotor with step skew, (d) rotor with teeth axial pairing.

based on rotor configurations are proposed. Fig. 6 shows the 3-D FEA model of PMFS machine with the three different rotor configurations.

A. Uniform Rotor with Optimal RPAW

The preceding analysis has been based on the rotor configuration with uniform poles, as shown in Fig.6 (b). The comprehensive results from Fig. 4 and Fig.5 show that the optimal RPAW is 1.9 for overall torque output and ripple torque performance. This configuration will be used as a benchmark for the subsequent techniques proposed.

B. Rotor Step Skewed

Among the rotor skewing techniques, RSS is relatively easy to fabricate since the skewing is arranged in discrete steps. By neglecting the axial interactions between the steps, the cogging torque of the machine with RSS can be derived by summing the cogging torque generated by each step. All the cogging torque harmonics can be eliminated except those are the multiples of the step number with the rotor equally skewed by the optimal angles [26]. There are essentially no even harmonics in cogging torque of the machine with 1.9 RPAW as shown in Fig.5, therefore, two discrete steps skewed by 3 degrees are deemed adequate to further reduce the cogging torque. The final configuration is shown as Fig. 6 (c).

C. Rotor Teeth Axial Pairing

Cogging torque can be artfully alleviated by constructing the

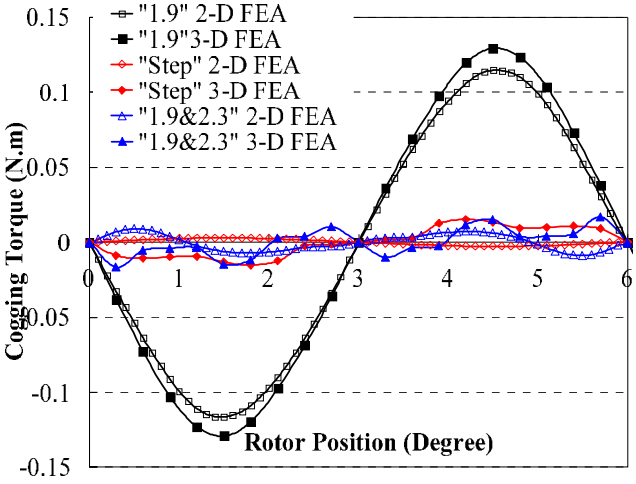

Fig. 7. Cogging torque waveforms with different rotor configurations from 2-D and 3-D FEA.

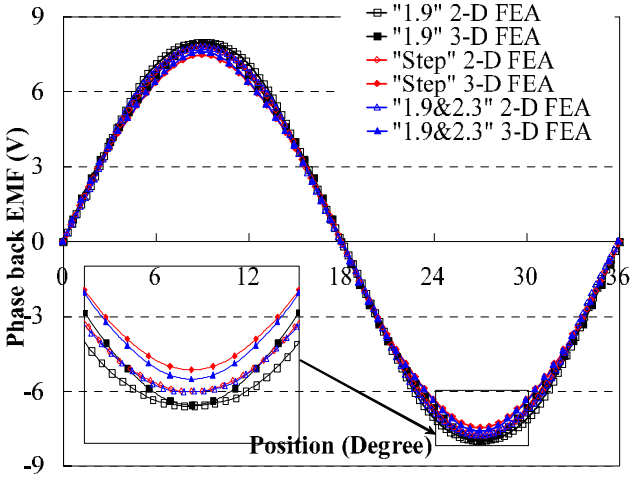

Fig. 8. Phase back EMF waveforms at 1000rpm with different rotor configurations from 2-D and 3-D FEA.

rotor stacks axially with different RPAW. The technique, called rotor teeth axial pairing (RTAP), can be seen as a machine made up of several different-axial-length machines with the same stator configuration axially conjoined together[21], [25]. The resultant cogging torque of the machine can be obtained by synthesizing the correponding cogging torques from each of the conjoining machines, provided there is negiligible axial interaction. By inspection of the result from Fig. 5, the cogging torques with 1.9 and 2.3 RPAW have opposite polarities but virtually equal P-P values. Consequently, cogging torque can be effectively counteracted by axially pairing two equal sectional length rotors with 1.9 and 2.3 RPAW. This rotor configuration is shown in Fig. 6 (d).

D. Rotor Teeth Axial Pairing

The 2-D FEA models have been developed for first order predictions based on simplified assumptions. However, to account for the end effects of the PMFS machine and the axial interactions of the rotor teeth, it is necessary to develop comprehensive 3-D FEA models for more accurate predictions for the cogging torque and phase back EMF. The 3-D FEA

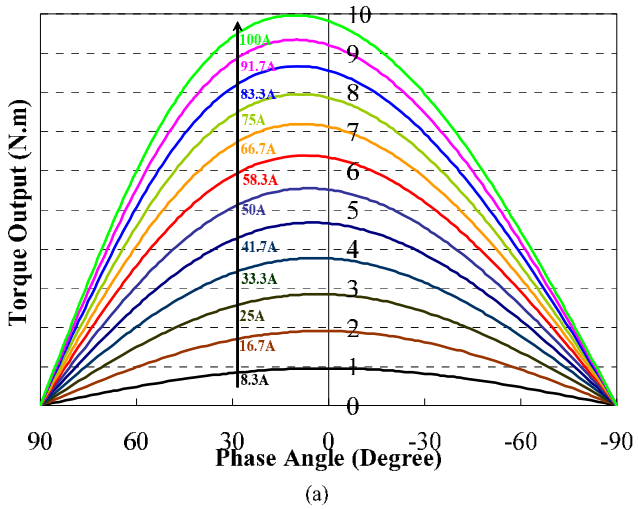

(a)

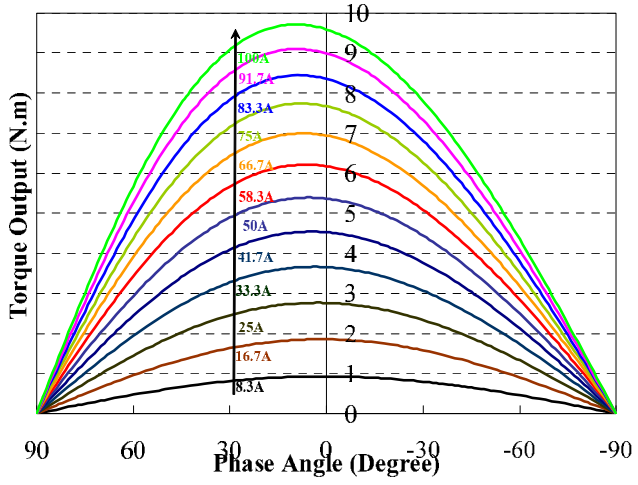

(b)

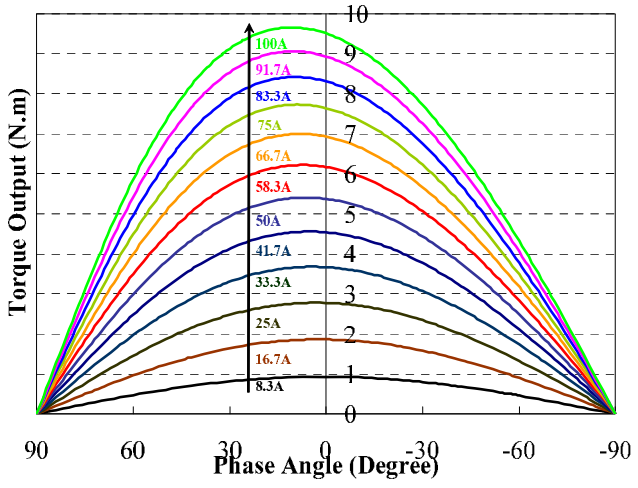

(c)

Fig. 9. Torque output with different current amplitude and phase advance angle, (a) uniform 1.9 RPAW, (b) step skew, (c) teeth axial pairing.

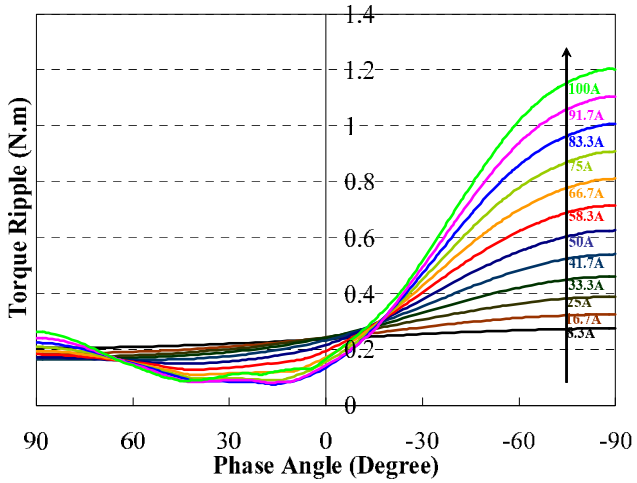

(a)

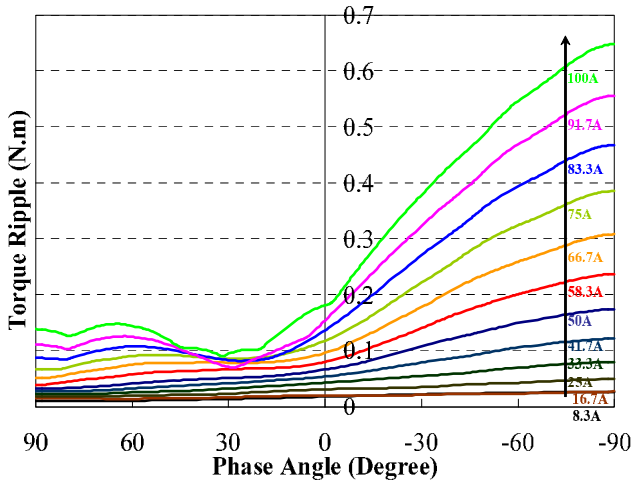

(b)

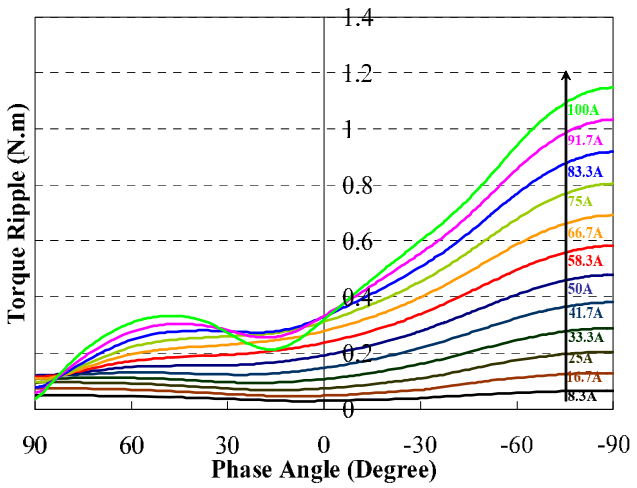

(c)

Fig. 10. P-P torque ripple with different current amplitude and phase advance angle, (a) uniform 1.9 RPAW, (b) step skew, (c) teeth axial pairing.

models in Fig.6 show the flux density distributions of the stator and the three rotor configurations under no load condition. The cogging torque profiles of the machine with different rotor configurations are estimated by synthesized 2-D and 3-D FEA, which are compared in Fig. 7. The results show the RSS and RTAP techniques can effectively suppress the cogging torque to very low levels compared against the benchmarking levels from the optimal 1.9 RPAW rotor configuration based on

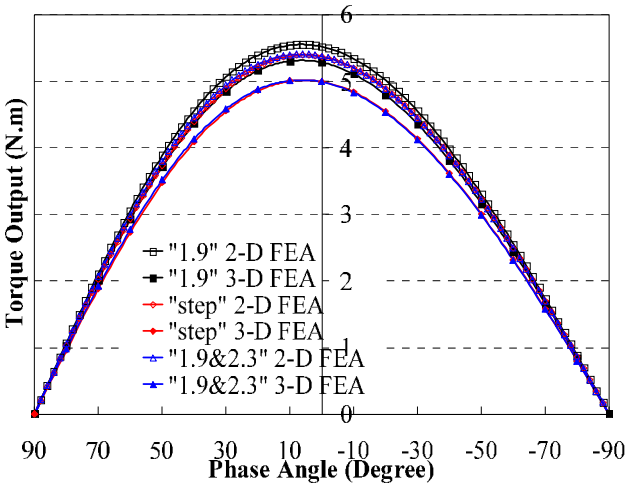

Fig. 11. Torque and phase advance angle characteristics with the three rotor configurations by 2-D and 3-D FEA.

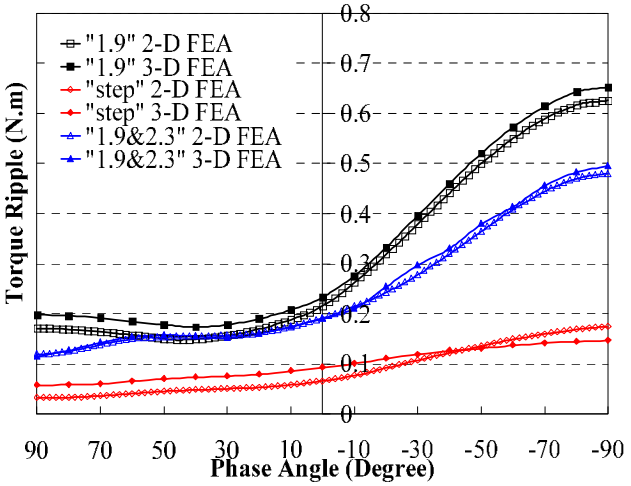

Fig. 12. P-P torque ripple and phase advance angle characteristics with different rotor configurations from 2-D and 3-D FEA.

between the 2-D and 3-D FEA results. Since the 3-D FEA results account for the end effects and axial interactions, the cogging levels are therefore higher than that of the 2-D FEA results, which ignore both effects. On the other hand, the corresponding back EMF waveforms at rated speed appear to be very similar and sinusoidal in all cases, as shown in Fig.8. Close inspection however shows the back EMF waveforms of the RSS and RTAP configurations are actually reduced and deteriorated to some extend from that of the optimal 1.9 RPAW configuration, leading to a reduction in output torque. This shows the usual performance tradeoff that is associated with cogging torque reduction methods.

V. Torque Analysis and Comparison with Different Rotor Configurations

The average torque and torque ripple of the machine for each rotor configuration are studied and compared in this section. The torque characteristics of the machine excited with various

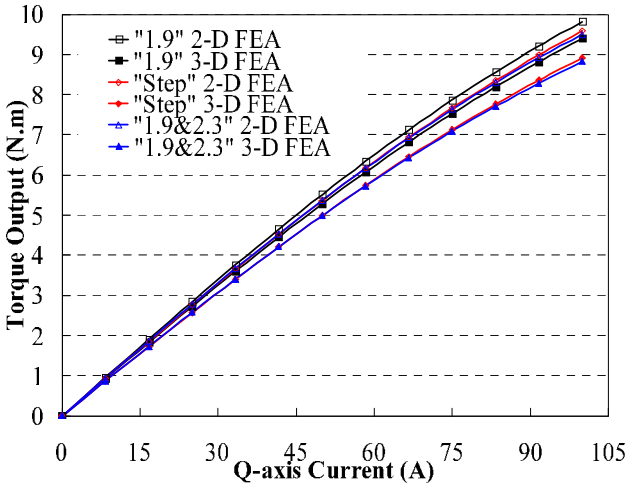

Fig. 13. Torque and current characteristics with different rotor configurations from 2-D and 3-D FEA.

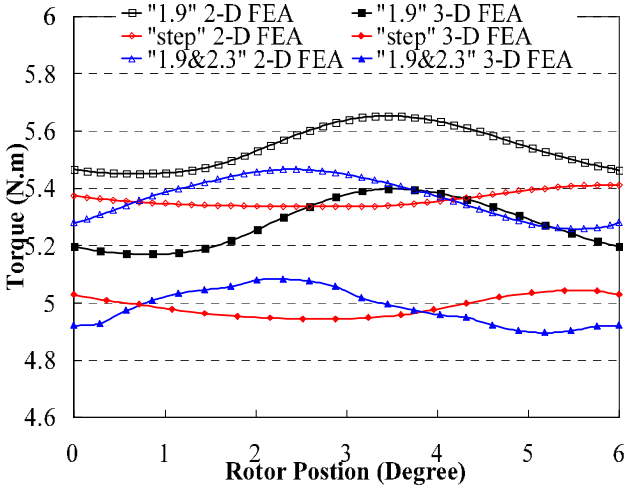

Fig. 14. Torque profiles with different rotor configurations from 2-D and 3-D FEA.

are analyzed using 2-D FEA. Without end effects and axial interactions considerations, the torque profiles of the RSS configuration can be expediently calculated using 2-D FEA results and phase advancing concept [26]. For the RTAP configuration, the resultant torque is obtained by synthesizing the 2-D FEA results from each conjoing rotor as in the previous section. Fig.9 shows the comprehensive results of the torque profiles of the three rotor configurations at different current excitations. The average torque reaches their maximums at around 8° phase advancing and gradually declines to zero as the phase angle approaches -90° or 90° for all three machines. It is also observed that the average torque output of the RSS and RTAP machines are somewhat depreciated. The corresponding P-P torque ripples are depicted in Fig. 10, which shows the torque ripples are much more significant with lagging phase angles for all three machines. The torque ripples generally increase with ascending current in all cases. However, the graphs in Fig.10 also show there are non-uniform variations at certain phase angles, as well as non-linearities when excessive current levels make the machine 'saturated'. However, the

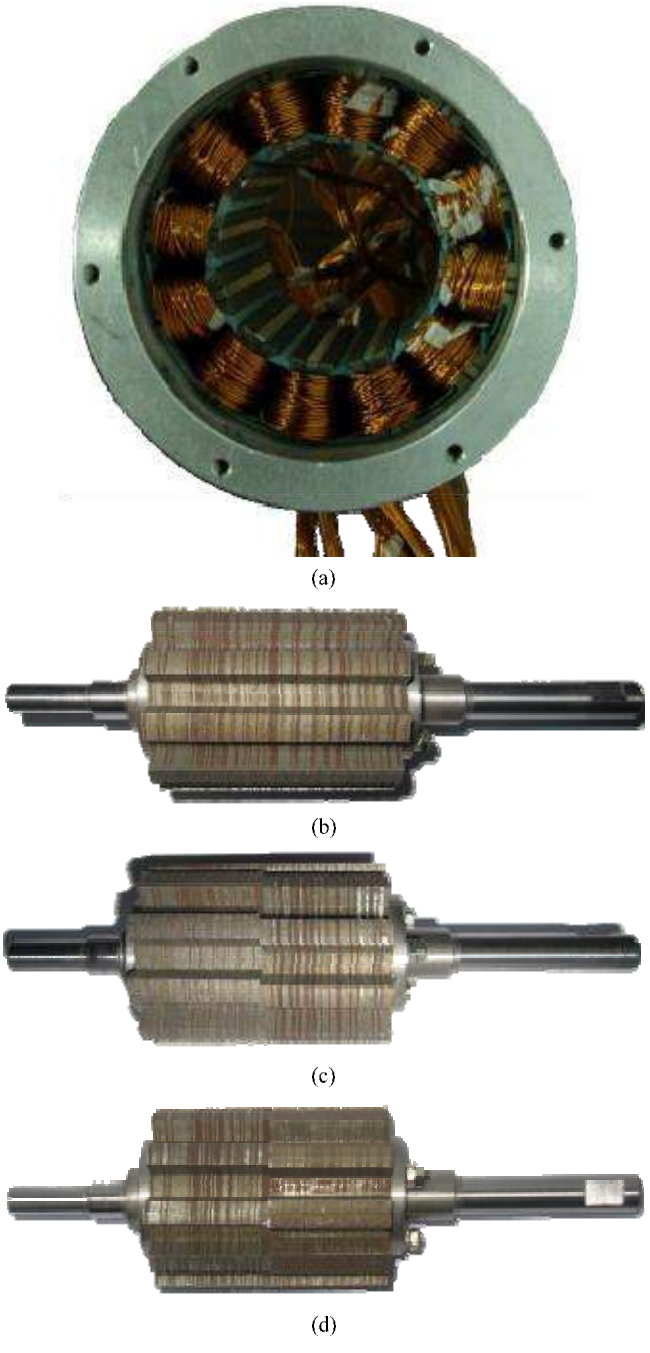

(a) (b) (c) (d)

Fig. 15. Prototype and experimental setup, (a) stator, (b) rotor with 1.9 RPAW, (c) rotor with step skew, (d) rotor with teeth axial pairing.

t ;

exceptionally subdued between -10˚ and 70˚ phase angles. For the RSS and RTAP configurations, the changes of the P-P torque ripple are almost negligible with leading phase angles when the currents are smaller than the rated value of 50A. The RSS configuration has the smallest torque ripples in all cases, whereas the RTAP configuration has smaller torque ripples than the 1.9 RPAW configuration at low current excitations (≤50A), but can have higher torque ripples in certain phase angle range at higher excitation current (≥50A).

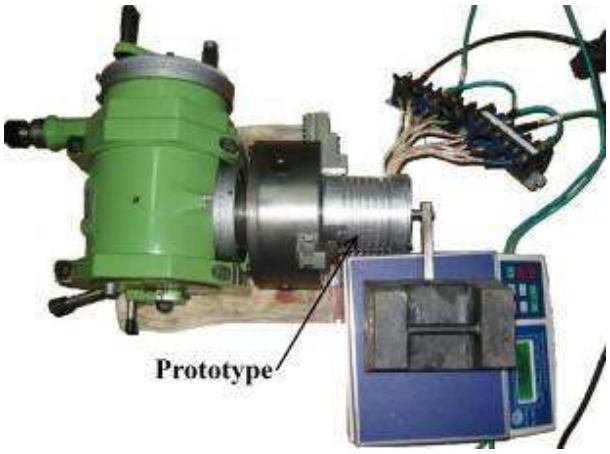

Fig. 16. Experimental setup.

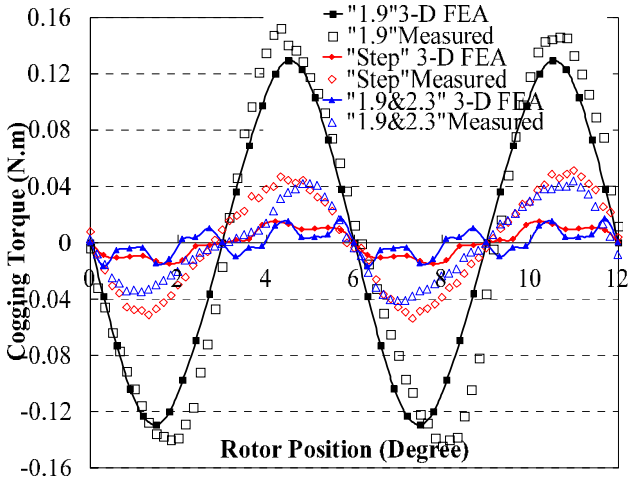

Fig. 17. Cogging torque waveforms with different rotor configurations from 3-D FEA and experiment.

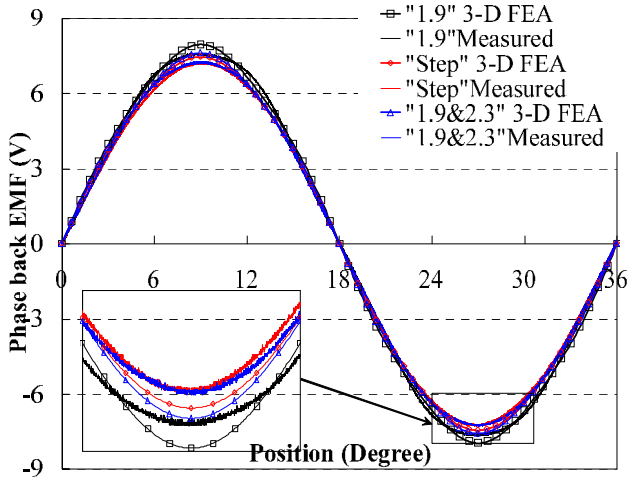

Fig. 18. Experimental test results of the prototype with axial magnets pairing.

above, 3-D FEA is comprehensively carried out with rated current 50A. The average torque and P-P torque ripple of the machines with different phase angles from 3-D FEA are shown and compared with the ones from 2-D FEA in Fig. 11 and Fig.

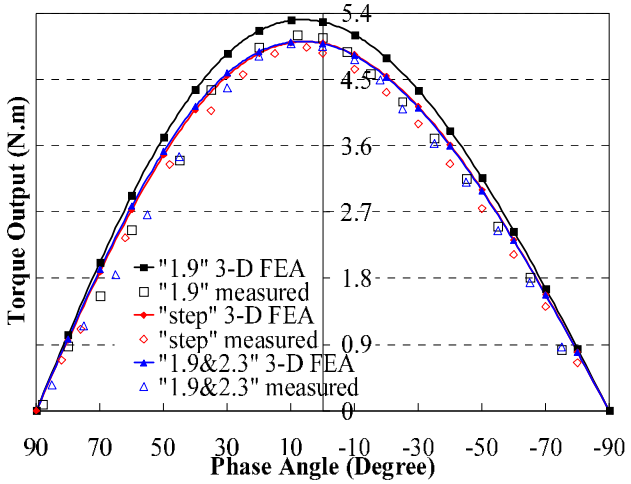

Fig. 19. Torque and phase advance angle characteristics with different rotor configurations from 3-D FEA and experiment.

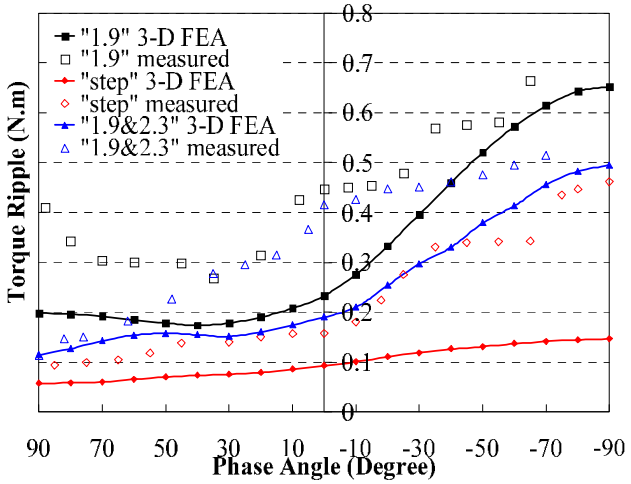

Fig. 20. P-P torque ripple and phase advance angle characteristics with different rotor configurations from 3-D FEA and experiment.

TABLE II
P-P COGGING TORQUE AND BACK EMF HARMONICS COMPARISONS

Machine	Parameters	2-D FEA	3-D FEA	Test
1.9 RPAW	P-P Cogging	0.23N·m	0.26N·m	0.30N·m
	1st EMF	8.03V	7.82V	7.72V
	5th EMF	0.151V	0.138V	0.146V
	7th EMF	0.0290V	0.0110V	0.00440V
RSS	P-P Cogging	0.0056N·m	0.030N·m	0.11N·m
	1st EMF	7.75V	7.39V	7.20V
	5th EMF	0.0564V	0.0697V	0.0120V
	7th EMF	0.0135V	0.0150V	0.0224V
RTAP	P-P Cogging	0.018N·m	0.034N·m	0.085N·m
	1st EMF	7.80V	7.48V	7.27V
	5th EMF	0.155V	0.110V	0.0614V
	7th EMF	0.0807V	0.00690V	0.0229V

d.

The 3-D FEA results of average torque are conceivably lower than the 2-D FEA ones due to consideration of the end effects and axial interactions, which also account for higher P-P torque ripple. Additionally, Fig. 13 illustrates the average torque output of the machines with different current excitations and 0° phase angle from both 2-D and 3-D FEA. The correlations between the average torque and current of the machine become

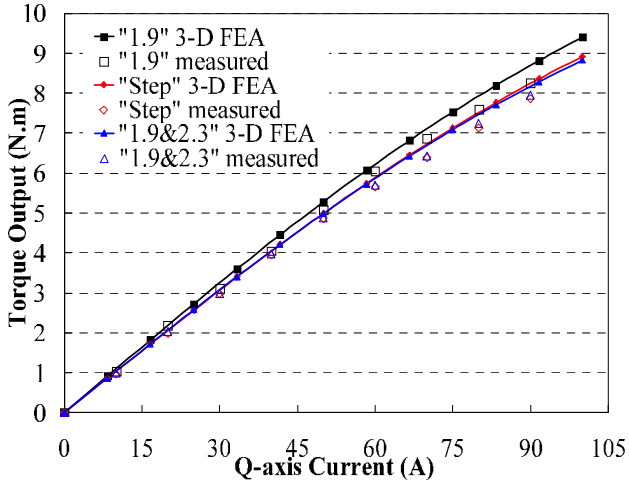

Fig. 21. Torque and current characteristics with different rotor configurations from 3-D FEA and experiment.

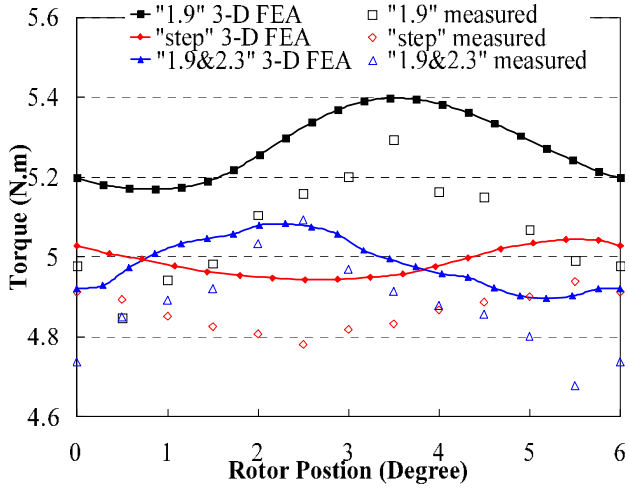

Fig. 22. Torque profiles with different rotor configurations from 3-D FEA and experiment.

severe saturations caused by high armature reaction. From Fig. 11 and Fig. 13, the RSS and RTAP machines share almost the same average torque output. Moreover, the corresponding torque profiles with 0° phase angle from 2-D and 3-D FEA are compared in Fig. 14, which shows the RTAP machine has the smallest torque ripple, while the RSS and 1.9 RPAW machines has similar torque ripples. It is also noted that that highest torque is delivered in the 1.9 RPAW machine.

VI. EXPERIMENTAL VALIDATIONS AND DISCUSSIONS

The stator and the three proposed rotor configurations are built for experimental validations of the FEA results. The prototypes and the experimental setup are shown in Fig. 15 and Fig. 16 respectively. The predicted cogging torque profiles of the machines from 3-D FEA are compared with the experimental results in Fig. 17. There are some noticeable deviations between the estimated and measured results, especially for the RSS and RTAP machines. The phase back EMF waveforms from the 3-D FEA and experimental tests at

1000rpm are compared as in Fig. 18, which shows the experimental ones are slightly smaller than the predicted. Moreover, the P-P cogging torque and dominant back EMF harmonics (1^{st}, 5^{th}, 7^{th}) are given in Table II for further comparisons. The FEA models are based on idealized machines with no mechanical tolerances and assembly deficiencies. In practice, it will be too costly, if not impossible, to build an ideal machine. Allowing also for errors due to experiments and software limitations, it is felt that these results from the FEA models and experimental tests are in satisfactory agreements. In addition, they also confirm that both the RSS and RTAP techniques can effectively reduce the cogging torque, albeit at the expense of small attenuations on the back EMF.

For the torque output and torque ripple tests, since the period of the torque pulsation is 6° (mechanical) due to machine symmetry as shown in Fig.14, it suffices to take 12 static torque measurements over a period of 6° (mech) by exciting the three phase winding with DC currents according to the rotor positions. The average torque and P-P torque ripple of the three proposed rotor configurations with different phase angles and rated current (50A) excitation from experiments are compared with 3-D FEA results in Fig. 19 and Fig. 20 respectively. There are relatively larger discrepancies between the predicted and measured results, compared with the previous comparison on cogging torque and back EMF. In addition to the previous explanations, there are further measurement uncertainties in the DC currents in the machine windings, and more importantly the machines have 10 rotor poles which would amplify any rotor position errors by 10 times when conducting the measurements. These factors potentially attribute to more significant experimental errors, as evident in the comparisons shown in Fig. 19 and Fig. 20. However, the experimental results further confirm the superiority of the RSS for its smallest torque pulsations among the three machines, whilst the P-P torque ripples in the 1.9 RPAW and RTAP machines are quite close with phase angles from -30° to 30°. The average torque output of the machines with different current excitations and 0° phase angle from both 3-D FEA and experimental tests are illustrated in Fig. 21, which show good agreements are achieved between the estimated and measured results, where latter are only very slightly smaller than the former. Moreover, the corresponding torque profiles with rated current excitation and 0° phase angle from 3-D FEA and experimental tests are compared in Fig. 22, and satisfactory agreements are again achieved.

From the above comprehensive analysis and comparisons, the RSS not only can significantly reduce the cogging torque but also greatly suppress the general torque ripple. Although the RTAP technique can effectively mitigate the cogging torque, it is not particularly effective to suppress the overall torque pulsation. However, it should be noted that both RSS and RTAP techniques compromise the torque output of the machine. It is therefore important to critically appraise the pros and cons of the technique to be deployed, in order to meet specific requirements of the application.

VII. Conclusion

Three rotor configurations have been proposed for cogging torque and torque ripple reduction of the PMFS ISG machine. The uniform rotor configuration is used as a design benchmark for the other RSS and RTAP configurations. Comprehensive FEA models have been developed for the machine's performance prediction. Experimental results have been carried out for the machine with three rotor configurations to validate the FEA models. The results show that the RSS and RTAP techniques are both very effective design to reduce the cogging torque in the proposed PMFS ISG. However, the RTAP method can only accomplish torque ripple improvement with low load conditions and will even increase torque pulsations with high load conditions while the RSS method can effectively suppress torque ripple with full-range loads. Careful selection is important for both cogging torque and torque ripple mitigations during the machine design stage.

Acknowledgment

The authors are gratefully indebted to C. Yuan of Wujiang Nanyuan Electical Co. China for the excellent manufacture of the prototypes, and Y. Wang, P. Li and L. L. Wang of Zhejiang University for the conduction of the experiments.

References

[1] S. E. Rauch, and L. J. Johnson, "Design principles of flux-switching alternators," *AIEE Trans., Power Apparatus Syst. Part III*, vol. 74, no. 3, pp. 1261-1268, Jan. 1955.

[2] E. Hoang, A. H. Ben-Ahmed, and J. Lucidarme, "Switching flux PM polyphased synchronous machines," in *Proc. 7th Eur. Conf. Power Electron. Appl.*, Sep. 1997, vol. 3, pp. 903-908.

[3] W. Fei, and J. X. Shen, "Novel permanent magnet switching flux motors," in *Proc. 41st Int. Universities Power Eng. Conf.*, Sep. 2006, vol. 2, pp. 729-733.

[4] W. Hua, M. Cheng, Z. Q. Zhu, and D. Howe, "Design of flux-switching permanent magnet machine considering the limitation of inverter and flux-weakening capability," in *Proc. IEEE Ind. Appl. Soc. 41st Annu. Meet.*, Oct. 2006, vol. 5, pp. 2403-2410.

[5] J. T. Chen, Z. Q. Zhu, and D. Howe, "Stator and rotor pole combinations for multi-tooth flux-switching PM brushless ac mahvines," *IEEE Trans. Magn.*, vol. 44, no. 12, pp. 4659-4667, Dec. 2008.

[6] Z. Q. Zhu, and J. T. Chen, "Advanced flux-switching permanent magnet brushless machines," *IEEE Trans. Magn.*, vol. 46, no. 6, pp. 1447-1453, Jun. 2010.

[7] Z. Q. Zhu, Y. Pang, D. Howe, S. Iwasaki, R. Deodhar, and A. Pride, "Analysis of electromagnetic performance of flux-switching PM machines by non-linear adaptive lumped parameter magnetic circuit model," *IEEE Trans. Magn.*, vol. 41, no. 11, pp. 4277-4287, Nov. 2005.

[8] Y. Chen, Z. Q. Zhu, and D. Howe, "Three-dimensional lumped parameter magnetic circuit model for analyzing single-phase flux-switching PM motor," *IEEE Trans. Ind. Appl.*, vol. 44, no. 6, pp. 1701-1710, Nov./Dec. 2008.

[9] B. L. J. Gysen, E. Ilhan, K. J. Meessen, J. J. H. Paulides, and E. A. Lomonova, "Modeling of flux switching permanent magnet machines with fourier analysis," *IEEE Trans. Magn.*, vol. 46, no. 6, pp. 1499-1502, Jun. 2010.

[10] E. Ilhan, B. L. J. Gysen, J. J. H. Paulides, and E. A. Lomonova, "Analytical hybrid model for flux switching permanent magnet machines," *IEEE Trans. Magn.*, vol. 46, no. 6, pp. 1762-1765, Jun. 2010.

[11] Y. Cheng, C. Pollock, and H. Pollock, "A permanent magnet flux switching motor for low energy axial fans," in *Proc. IEEE Ind. Appl. Soc. 40th Annu. Meet.*, Oct. 2005, vol. 3, pp. 2168-2175.

[12] Y. Amara, E. Hoang, M. Gabsi, M. Lecrivain, and S. Allano, "Design and comparison of different flux-switch synchronous machines for an aircraft oil breather application," *Eur. Trans. Elect. Power,* vol. 15, no. 6, pp. 497-511, Nov./Dec. 2005.

[13] Z. Q. Zhu, J. T. Chen, and D. Howe, "Analysis of a novel multi-tooth flux-switching PM brushless ac machine for high torque direct-drive applications," *IEEE Trans. Magn.*, vol. 44, no. 11, pp. 4313-4316, Nov. 2008.

[14] W. Fei, P. C. K. Luk, J. X. Shen, and Y. Wang, "A novel outer-rotor PM flux-switching machine for urban electric vehicle propulsion," in *Proc. 3rd Int. Conf. Power Electon. Syst. Appl.*, May 2009, pp. 1-6.

[15] A. S. Thomas, Z. Q. Zhu, R. L. Owen, G. W. Jewell, and David Howe, "Multiphase flux-switching permanent-magnet brushless machine for aerospace application," *IEEE Trans. Ind. Appl..*, vol. 45, no. 6, pp. 1071-1981, Nov./Dec. 2009.

[16] A. Walker, P. Anpalahan, P. Coles, M. Lamperth, and D. Rodgert, "Automotive integrated starter generator," in *Proc. 2nd IEE Power Electron, Machines and Drives Conf.*, Apr. 2004, vol. 1, pp. 46-48.

[17] Z. X. Fang, Y. Wang, J. X. Shen, and Z. W. Huang, "Design and analysis of a novel flux-switching permanent magnet integrated-starter-generator," in *Proc. 6th IEE Power Electron, Machines and Drives Conf.*, Apr. 2008, pp. 106-110..

[18] W. Hua, and M. Cheng, "Cogging torque reduction of flux-switching permanent magnet machines without skewing," in *Proc. 11th Int. Electrical Machines and Systems Conf.*, Oct. 2008, pp. 3020-3025.

[19] Z. Q. Zhu, A. S. Thomas, J. T. Chen, and G. W. Jewell, "Cogging torque in flux-switching permanent magnet machines," *IEEE Trans. Magn.*, vol. 45, no. 10, pp. 4708-4711, Oct. 2009.

[20] M. J. Jin, Y. Wang, J. X. Shen, P. C. K. Luk, W. Fei, and C. F. Wang, "Cogging torque suppression in a permanent-magnet flux-switching integrated-starter-generator," *IET Electr. Power Appl.*, vol. 4, no. 8, pp. 647-656, Sep. 2010.

[21] Y. Wang, M. J. Jin, W. Fei, and J. X. Shen, "Cogging torque reduction in PM flux-switching machines by rotor teeth axial pairing," *IET Electr. Power Appl.*, vol. 4, no. 7, pp. 500-506, Aug. 2010.

[22] H. Jia, M. Cheng, W. Hua, W. Zhao, and W. Li, "Torque ripple suppression in flux-switching PM motor by harmonic current injection based on voltage space-vector modulation," *IEEE Trans. Magn.*, vol. 46, no. 6, pp. 1527-1530, Jun. 2010.

[23] W. Hua, M. Cheng, Z. Q. Zhu, and D. Howe, "Analysis and optimization of back-emf waveform of a flux-switching PM motor," *IEEE Trans. Energy Conversion*, vol. 23, no. 3, pp. 727-733, Sep. 2008.

[24] W. Hua, M. Cheng, "Inductance characteristics of 3-phase flux-switching permanent magnet machine with doubly-salient structure," in *Proc. 5h Int. Power Electon. And Motion Control Conf.*, Aug. 2006, vol. 3, pp. 1-5.

[25] W. Fei, and P. C. K. Luk, "A new technique of cogging torque suppression in direct-drive permanent magnet brushless machines," *IEEE Trans. Ind. Appl..*, vol. 46, no. 4, pp. 1332-1340, Jul./Aug. 2010.

[26] N. Bianchi, and S. Bolognani, "Design techniques for reducing the cogging torque in surface-mounted PM motors," *IEEE Trans. Ind. Appl..*, vol. 38, no. 5, pp. 1259-1265, Sep./Oct. 2002.

[27] R. Islam, I. Husain, A. Fardoun, and K. Mclaughlin, "Permanent-magnet synchronous motor magnet designs with skewing for torque ripple and cogging torque reduction," *IEEE Trans. Ind. Appl..*, vol. 45, no. 1, pp. 152-160, Jan./Feb. 2009.

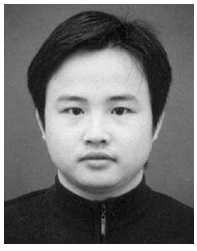

W. Fei was born in Zhejiang, China, 1981. He received the B.Eng. and M.Eng. degrees in electrical engineering from Zhejiang University, Hangzhou, China, in 2004 and 2006, respectively. He is currently working towards Ph.D. degree with Power and Drive Systems Group, Cranfield Defence and Security, Cranfield University, U. K.

His current research interests include design and applications of permanent-magnet machines and drives.

P. C. K. Luk (M'92-SM'08) was born in Hongkong, 1960. He received his high diploma with merit from Hongkong Polytechnic University in 1983, MPhil from Sheffield University in 1989, and Ph.D. from Glamorgan University in 1992, all in electrical engineering.

He started his career as assistant engineer at GEC (HK) and then as researcher at the Industrial Centre of PolyU. Since 1988, he had held academic positions at the universities of Glamorgan, Robert Gordon and Herfordshire. He joined Cranfield University as senior lecture in 2002. Currently, his the head of Power and Drive Systems Group. His current main research interests are in electrical drives for electric vehicles and renewable energy applications.

J. X. Shen (M'98-SM'03) was born in Huzhou, China, in 1969. He received the B.Eng. and M.Sc. degrees from Xi'an Jiaotong University, Xi'an, China, in 1991 and 1994, respectively, and the Ph.D. degree from Zhejiang University, Hangzhou, China, in 1997, all in electrical engineering.

He was with Nanyang Technological University, Singapore (1997–1999), the University of Sheffield, Sheffield, U.K. (1999–2002), and IMRA Europe SAS, U.K. Research Centre, Brighton, U.K. (2002–2004). Since 2004, he has been a professor of electrical engineering at Zhejiang University. He has published more than 110 papers and obtained 17 patents. He received a Prize Paper Award from the IEEE Industry Applications Society in 2003, and a Best Paper Award from EVER-Monaco in 2010. His main research interests include topologies, control and applications of permanent-magnet machine drives.

B. Xia was born in Guilin, China, in 1985. He received the B.Eng. degree in electrical engineering from Zhejiang University, Hangzhou, China, in 2008. He is working towards the Master's degree in electrical engineering at Zhejiang University.

His current research interests include design and applications of permanent-magnet machines and drives.

Y. Wang was born in Zhejiang, China, in 1983. He received the B.Eng. degree in electrical engineering from Zhejiang University, Hangzhou, China, in 2006. He is now working towards the Ph. D. degree in electrical engineering at Zhejiang University.

His main research interests include topologies, control and applications of flux switching permanent magnet machine drives.